HHS Public Access

Author manuscript

Biochim Biophys Acta. Author manuscript; available in PMC 2019 March 01.

Published in final edited form as:

Biochim Biophys Acta. 2018 March ; 1864(3): 819–830. doi:10.1016/j.bbadis.2017.12.013.

Protective effect of genetic deletion of pannexin1 in experimental mouse models of acute and chronic liver disease

Joost Willebrords[a,*], **Michaël Maes**[a,*], **Isabel Veloso Alves Pereira**[b], **Tereza Cristina da Silva**[b], **Veronica Mollica Govoni**[b], **Valéria Veras Lopes**[b], **Sara Crespo Yanguas**[a], **Valery I. Shestopalov**[c], **Marina Sayuri Nogueira**[d], **Inar Alves de Castro**[d], **Anwar Farhood**[e], **Inge Mannaerts**[f], **Leo van Grunsven**[f], **Jephte Akakpo**[g], **Margitta Lebofsky**[g], **Hartmut Jaeschke**[g], **Bruno Cogliati**[b,#], and **Mathieu Vinken**[a,#]

[a]Department of *In Vitro* Toxicology and Dermato-Cosmetology, Faculty of Medicine and Pharmacy, Vrije Universiteit Brussel, Laarbeeklaan 103, 1090 Brussels, Belgium

[b]Department of Pathology, School of Veterinary Medicine and Animal Science, University of São Paulo, Av. Prof. Dr. Orlando Marques de Paiva 87, 05508-270, São Paulo, Brazil

[c]Bascom Palmer Eye Institute, Department of Ophthalmology, University of Miami Miller School of Medicine, 1638 NW 10th Avenue, 33136 Miami, Florida, United States

[d]Department of Food and Experimental Nutrition, Faculty of Pharmaceutical Sciences, University of São Paulo, Av. Prof. Lineu Prestes 580, 05508-270 São Paulo, Brazil

[e]Department of Pathology, St. David's North Austin Medical Center, 601E 15th Street, 78701 Austin, United States of America

[f]Department of Liver Cell Biology, Faculty of Medicine and Pharmacy, Vrije Universiteit Brussel, Laarbeeklaan 103, 1090 Brussels, Belgium

[g]Department of Pharmacology, Toxicology and Therapeutics, University of Kansas Medical Center, 3901 Rainbow Blvd, 66160 Kansas City, United States of America

Correspondence to: Mathieu Vinken.

[*]equally contributing first authors.

[#]equally contributing senior authors.

Joost Willebrords: joost.willebrords@vub.be; +32 2 477 45 87
Sara Crespo Yanguas: sara.crespo.yanguas@vub.ac.be; +32 2 477 45 87
Michaël Maes: michael.mc.maes@vub.be; +32 2 477 45 87
Mathieu Vinken: mvinken@vub.ac.be; +32 2 477 45 87
Bruno Cogliati: bcogliati@usp.br; +55 11 30 91 12 00
Isabel Veloso Alves Pereira: isabelveloso@gmail.com; +55 11 30 91 12 00
Tereza Cristina da Silva: terezacs@usp.br; +55 11 30 91 12 00
Veronica Mollica Govoni: veronica.mgovoni@gmail.com; +55 11 30 91 12 00
Valéria Veras Lopes: valeria.veras95@gmail.com; +55 11 30 91 12 00
Valery I. Shestopalov: vshestopalov@miami.edu; +1 305 547 3680
Marina Sayuri Nogueira: masayuri.nogueira@gmail.com; +55 11 30 91 36 30
Inar Alves de Castro: inar@usp.br; +55 11 30 91 36 30
Anwar Farhood: farhood.a.i@gmail.com; +1 512 324 7516
Inge Mannaerts: inmannae@vub.ac.be; +32 2 477 44 07
Leo Van Grunsven: lvgrunsv@vub.ac.be; +32 2 477 44 07
Jephte Akakpo: jakakpo@kumc.edu; +1 913 588 9184
Margitta Lebofsky: mlebofsky@kumc.edu; +1 913 588 9184
Hartmut Jaeschke: hjaeschke@kumc.edu; +1 913 588 7969

Conflict of interest

The authors report no declarations of interest.

Abstract

Pannexins are transmembrane proteins that form communication channels connecting the cytosol of an individual cell with its extracellular environment. A number of studies have documented the presence of pannexin1 in liver as well as its involvement in inflammatory responses. In this study, it was investigated whether pannexin1 plays a role in acute liver failure and non-alcoholic steatohepatitis, being prototypical acute and chronic liver pathologies, respectively, both featured by liver damage, oxidative stress and inflammation. To this end, wild-type and pannexin1$^{-/-}$ mice were overdosed with acetaminophen for 1, 6, 24 or 48 hours or were fed a choline-deficient high-fat diet for 8 weeks. Evaluation of the effects of genetic pannexin1 deletion was based on a number of clinically relevant read-outs, including markers of liver damage, histopathological analysis, lipid accumulation, protein adduct formation, oxidative stress and inflammation. In parallel, in order to elucidate molecular pathways affected by pannexin1 deletion as well as to mechanistically anchor the clinical observations, whole transcriptome analysis of liver tissue was performed. The results of this study show that pannexin1$^{-/-}$ diseased mice present less liver damage and oxidative stress, while inflammation was only decreased in pannexin1$^{-/-}$ mice in which non-alcoholic steatohepatitis was induced. A multitude of genes related to inflammation, oxidative stress and xenobiotic metabolism were differentially modulated in both liver disease models in wild-type and in pannexin1$^{-/-}$ mice. Overall, the results of this study suggest that pannexin1 may play a role in the pathogenesis of liver disease.

Keywords

Acute liver failure; non-alcoholic steatohepatitis; pannexin; hepatotoxicity; inflammation

1. Introduction

Pannexins (Panx) are transmembrane proteins that constitute channels connecting the cytosol of a cell with its extracellular environment [1]. The Panx family consists of 3 members (Panx1–3), of which 1 or more have been detected in every mammalian organ [2, 3]. Among those, Panx1 has been most extensively studied. When open, Panx1 channels form communication pathways that allow the passage of small and hydrophilic molecules, including adenosine triphosphate (ATP) [4]. The opening of these Panx1 channels seems to correlate with the activation and/or perpetuation of inflammation [5, 6], as they assist in the processing and release of the pro-inflammatory cytokines interleukin (IL)-1β and IL-18 [7] through activation of the NACHT, LRR and PYD domains-containing protein 3 (NALP3) inflammasome, a multiprotein complex involved in innate immunity and coded by the NLRP3 gene [8, 9]. Panx1 channels also drive the stimulation and migration of leukocytes, and seem to play a role in the recruitment of neutrophils [10, 11]. Furthermore, Panx1 channels participate in the dissemination of cell death by releasing so-called “find-me” signals from apoptotic cells in order to recruit phagocytes [12]. Inflammation accompanies a wide spectrum of acute and chronic diseases, including acute liver failure and non-alcoholic steatohepatitis (NASH).

Drug-induced liver injury is the leading cause of acute liver failure in Western countries. A majority of the clinical cases of acute liver failure results from either accidental or

intentional overdose of acetaminophen (APAP, paracetamol), a readily available analgesic and antipyretic drug [13]. In case of APAP overdose, a substantial amount of APAP is metabolized by cytochrome P450 2E1 (Cyp2E1), yielding the reactive metabolite *N*-acetyl-*p*-benzoquinone imine (NAPQI), which depletes the glutathione (GSH) pool and that gives rise to deleterious APAP-protein adducts [14]. As a consequence, impaired mitochondrial respiration and oxidative stress are triggered, and accompanied by the onset of massive hepatocyte cell death as well as the induction of an inflammatory response [15]. Increased hepatic Panx1 levels have been observed during APAP-induced acute liver failure [11] as well as in experimentally induced NASH in mouse, the latter being paralleled by activation of the NALP3 inflammasome [5, 16]. Along the same line, previous work from our group showed that pharmacological inhibition of Panx1 channel opening alleviates liver injury after APAP overdosing of mice [11].

Non-alcoholic fatty liver disease (NAFLD) is currently the most common chronic liver disease in Western countries [17]. NAFLD embodies a broad range of liver diseases, of which 25–30% of liver steatosis patients progress to NASH and approximately 3% of NASH patients develop liver cancer [18]. The mechanisms underlying the development and progression of NASH are complex and multifactorial. Indeed, the pathogenesis of NASH is currently displayed in a multiple-hit model that involves insulin resistance, nutritional factors, gut microbiota, inflammatory liver environment, oxidative stress and genetic factors [19]. In NASH, hepatic lipid accumulation is compensated by increased mitochondrial oxidation, causing an overproduction of free radicals, such as reactive oxygen species [20]. Reactive oxygen species are able to directly deplete anti-oxidative molecules, including GSH, and to inhibit the activities of anti-oxidative enzymes, such as superoxide dismutase (SOD), GSH reductase (GR), GSH peroxidase (GPx) and catalase [21]. In fact, NASH mice and human NASH patients exhibit decreased GSH content, SOD and catalase activities [22, 23]. Moreover, cholesterol can initiate and propagate inflammation and subsequent fibrosis in NASH [24]. Increased hepatic cholesterol levels in NASH are caused by extensive dysregulation of cholesterol homeostasis through excess dietary cholesterol, increases in hepatic synthesis or decreased excretion [24]. This overload of cholesterol may subsequently form cholesterol crystals, activate Kupffer cells [25] and trigger the NLRP3 inflammasome [26].

The present study was set up to gain more insight into the involvement of Panx1 in NASH and acute liver failure. For this purpose, wild-type (WT) and whole body Panx1$^{-/-}$ mice were overdosed with APAP, or fed a choline-deficient high-fat diet (CHFD) or normal diet (ND). The resulting acute liver failure and NASH responses were evaluated based on several clinically relevant parameters combined with mechanistic microarray analysis.

2. Materials and methods

2.1 Animals and treatment

BALB/c mice were kept under controlled environmental conditions with free access to food and water in the animal facility of the Faculty of Pharmacy and Medicine at Vrije Universiteit Brussel-Belgium. Hepatic stellate cells (HSCs), liver sinusoidal endothelial cells (LSECs), Kupffer cells and hepatocytes were isolated as previously described [27]. Panx1$^{-/-}$

mice were kindly provided by Dr. Shestopalov and were generated as described elsewhere [28]. 8-week old male C57BL/6 WT and Panx1$^{-/-}$ mice were housed in the animal facility of the Department of Pathology, School of Veterinary Medicine and Animal Science of the University of São Paulo-Brazil. The animals were kept in a room with ventilation, relative humidity, controlled temperature and light/dark cycle 12:12, and were given water and balanced diet *ad libitum.* In a first set of experiments, mice were starved 15–16 hours *prior* to APAP (Sigma, USA) or vehicle administration. APAP was dissolved in saline, slightly heated and injected (30–37°C) intraperitoneally at 300 mg/kg body weight, after which animals regained free access to food. Mice were euthanized at the start of the experiment or 1, 6, 24 or 48 hours after APAP injection. In a second set of experiments, mice were fed a CHFD (35% total fat and 54% trans fatty enriched) (Rhoster, Brazil) or ND for 8 weeks. All animals were euthanized by isoflurane-induced anesthesia and exsanguination during sampling. Blood samples were drawn into heparinized syringes and centrifuged for 10 minutes at 1503*xg*, and serum was stored at −80°C. Liver fragments were fixed in phosphate-buffered formalin or snap-frozen in liquid nitrogen with storage at −80°C. This study has been approved by the Committee on Bioethics of the School of Veterinary Medicine and Animal Science of the University of São Paulo-Brazil (Protocol number 9999100314) and all animals received humane care according to the criteria outlined in the "Guide for the Care and Use of Laboratory Animals".

2.2 Examination of liver histopathology

Liver tissue samples were fixed in 10% phosphate-buffered formalin for 24 hours and embedded in paraffin wax. Samples were cut into 5 μm sections and stained with hematoxylin and eosin for evaluation of liver damage as described previously [29]. The percentage of necrosis was estimated by evaluating the number of microscopic fields with necrosis compared to the cross-sectional areas of the entire section. Steatosis (0–3), hepatocellular ballooning (0–2) and lobular inflammation (0–3) were scored as explained elsewhere [30] and the NAFLD activity score (NAS) (0–8) was calculated.

2.3 Analysis of serum aminotransaminases, serum and liver triglycerides and cholesterol

Liver tissue was homogenized in 1 mL 2:1 chloroform/methanol solution and shaken for 1 hour in a Thermomixer (Eppendorf, Germany) at 22°C. Samples were centrifuged for 10 minutes at 5000*xg*, after which the supernatant was isolated. Next, 200 μL distilled water was added and samples were centrifuged for 5 minutes at 8000*xg*. The bottom phase was dried overnight at 37°C. *Prior* to analysis, lipids were dissolved in 400 μL butanol (Sigma, USA). Serum activity of alanine (ALT) and aspartate (AST) aminotransferase as well as serum and liver triglycerides and cholesterol were measured by a chemistry analyser after appropriate dilution if necessary (Labmax 240, Labtest, Brazil). Results were expressed in IU/L for AST and ALT, mg/dL for serum triglycerides and cholesterol, and μg/mg for liver triglycerides and cholesterol.

2.4 Analysis of liver oxidative stress

SOD, GPx, GR and catalase activities in liver homogenates were determined as explained previously [31]. Results were expressed as U/mg protein. GSH and glutathione disulfide (GSSG) levels in liver tissue were measured using a modified Tietze assay [32]. In essence,

frozen liver tissue was homogenized in 3% sulfosalicylic acid/ethylendiaminetetraacetic acid and centrifuged at 18000*xg* for 5 minutes at 4°C to remove precipitated proteins. After further dilution with potassium phosphate buffer, samples were assayed with a cycling reaction utilizing GSH reductase and dithionitrobenzoic acid. Measurement of GSSG was performed using the same method after trapping and removal of GSH with *N*-ethylmaleimide and removal by solid phase extraction. GSSG content was expressed as GSH equivalents.

2.5 Analysis of liver protein adducts

APAP-protein adducts were measured by high-pressure liquid chromatography with electrochemical detection as described elsewhere [33] with some modifications [34]. Briefly, low molecular weight compounds were removed *via* Bio-spin 6 columns (Bio-Rad, USA) and the protein fraction was subsequently digested with proteases to liberate APAP-cysteine conjugates. The protein-derived APAP-cysteine conjugates were quantified and normalized to protein concentration in the original samples.

2.6 Analysis of liver inflammatory markers

Levels of inflammatory markers were determined in liver homogenates using a Mouse Inflammation Antibody Array (Abcam, UK) following the manufacturer's instructions. Briefly, membranes spotted with capture antibodies were incubated while shaking with blocking buffer for 30 minutes at room temperature. Subsequently, membranes were incubated overnight at 4°C with 250 μg protein diluted in 1 mL blocking buffer. Membranes were washed, incubated with biotin-conjugated anti-cytokines for 2 hours at room temperature, washed again and incubated with horseradish peroxidase-conjugated streptavidin for 2 hours at room temperature. Following washing, proteins were detected by means of enhanced chemiluminescence and visualized with a Chemidoc™ MP system (Bio-Rad, USA). Semi-quantitative results were obtained after densitometric analysis using Image Lab 5.0 software (Bio-Rad, USA), were expressed as arbitrary units normalized to immunoglobulin G, which serves as a positive control, and were presented as relative alterations compared to control animals.

2.7 Immunoblot analysis

Immunoblot analysis of liver extracts was performed as previously described [35]. Nitrocellulose membranes were incubated overnight at 4°C with primary antibody directed to Cyp2e1 (1/250 dilution), SOD (1/500 dilution), GR (1/250 dilution), GPx (1/1000 dilution) and catalase (1/100 dilution) (Sigma, USA) followed by incubation for 1 hour at room temperature with appropriate secondary antibody (1/250 dilution for catalase, 1/500 dilution for Cyp2e1 and GR and 1/1000 dilution for SOD and GPx) (Dako, Denmark). Densitometric analysis was performed using Image Lab 5.0 software (Bio-Rad, USA). For semi-quantification purposes, signals were normalized against total protein, measured by activation and quantification of the stain-free loading on Stain-Free™ precast gels, and expressed as relative alterations compared to WT ND animals for NASH and WT untreated animals for APAP.

2.8 Gene expression analysis

Total RNA was extracted from liver tissue or liver cells using a GenElute™ Mammalian Total RNA Purification Miniprep Kit and an On-Column DNase I Digestion Set according to the manufacturer's instructions. Purity and quantification of isolated RNA were measured spectrophotometrically using a Nanodrop® ND-100 Spectrophotometer (Thermo Scientific, USA). Subsequently, 2 μg RNA was reversely transcribed into cDNA with an iScript™ cDNA Synthesis Kit (Bio-Rad, USA) using an iCycler iQ™ (Bio-Rad, USA) followed by cDNA purification using a GenElute™ PCR Clean-Up Kit. cDNA products were quantitatively amplified by means of Taqman probes and primers (Applied Biosystems, USA) targeted towards *Panx1*, *Cd36*, *Cd68* and *Cxcl9* and candidate reference genes (Table 1). All samples were analyzed in duplicate. Each run included a serial dilution of a pooled cDNA mix from all cDNA samples and 2 no-template controls to estimate the quantitative polymerase chain reaction efficiency. For reverse transcription quantitative real-time polymerase chain reaction (RT-qPCR) analysis, a mix was prepared containing TaqMan® Fast Advanced Master Mix (Applied Biosystems, USA), Assay-on-Demand™ Gene Expression Assay Mix (Applied Biosystems, USA) and cDNA diluted in nuclease-free water. The qPCR conditions, using a StepOnePlus™ real-time PCR system (Life Technologies, USA), included incubation for 20 seconds at 95°C followed by 40 cycles of denaturation for 1 second at 95°C and annealing for 20 seconds at 60°C. Efficiency was estimated by the StepOne Plus™ system's software and only data with PCR efficiency between 90 and 110% were used. Stable candidate reference genes for normalization purposes were identified out of a pool of 6 genes as determined by geNorm using the qbase+ software (Biogazelle, Belgium). The resulting ΔCq values of the test samples were normalized to those of the calibrator samples, yielding ΔΔCq values. Relative alterations (fold change) in RNA levels were calculated according to the Livak $2^{-\Delta\Delta Cq}$ formula [36].

2.9 Whole transcriptome analysis

After RNA extraction, integrity was analyzed by microfluidic analysis by means of an Agilent 2100 Bioanalyzer (Agilent Technologies, USA). A total of 100 ng RNA *per* sample was amplified with a Genechip 3′ IVT Express Kit, thereby following the manufacturer's instructions (Affymetrix, Germany). Amplified RNA was purified with magnetic beads and 15 mg biotin-amplified RNA was treated with the fragmentation reagent. Subsequently, 12.5 μg fragmented amplified RNA was hybridized to Affymetrix Clariom™ D mouse arrays and placed in a Genechip Hybridization Oven-645 (Affymetrix, Germany) rotating at 60 rpm at 45°C for 16 hours. Thereafter, the arrays were washed on a Genechip Fluidics Station-450 (Affymetrix, Germany) and stained with an Affymetrix HWS kit. The chips were scanned with an Affymetrix Gene-Chip Scanner-3000-7G and quality control matrices were confirmed with Affymetrix GCOS software following the manufacturer's guidelines. Background correction, summarization and normalization of all data were done with Expression Console and Affymetrix Transcriptome Analysis Console Software.

2.10 Statistical analysis

The number repeats (n) for each analysis varied and is specified in the discussion of the results. All data were expressed as mean ± standard error of mean (SEM). Results were

statistically processed by 1-way analysis of variance with *post hoc* Bonferroni correction. All data were processed using GraphPad Prism6 software, with probability (p) values of less than 0.05 considered as significant.

3. Results

3.1 Panx1 expression in liver

A number of reports have described the presence of Panx1 in liver, particularly in hepatocytes and Kupffer cells [6, 37, 38]. In order to study the Panx1 expression pattern in these and other liver cells, HSCs, hepatocytes, Kupffer cells and LSECs were isolated from untreated mice (n=5), followed by analysis of Panx1 RNA levels. Panx1 RNA was found in HSCs, hepatocytes and Kupffer cells, but not in LSECs of healthy animals (Fig. 1A). Importantly, Panx1 RNA expression was increased in APAP-treated mice (n=5) after 6 ($p<0.01$) and 24 hours ($p<0.0001$) compared to saline control (n=5) (Fig. 1B) as well as in CHFD-fed mice ($p<0.01$) (n=10) in comparison with ND (n=9) counterparts after 8 weeks.

3.2 Effects of Panx1 deficiency on liver injury

A single dose of 300 mg/kg APAP is well known to cause severe hepatocellular injury, which can be detected by massive necrosis and extensive increased serum ALT and AST activities [11]. This was confirmed in the current study, where liver damage became manifested about 6 hours after APAP injection in the different experimental groups. Except for the 6 hour time point, no significant alterations in necrotic areas were found between APAP-treated WT and Panx1$^{-/-}$ mice (Fig. 2A), although ALT and AST activities were significantly reduced after 6 (ALT $p<0.001$; AST $p<0.05$) and 24 hours (ALT $p<0.0001$; AST $p<0.0001$) in APAP-treated Panx1$^{-/-}$ mice (n=7) compared to their WT counterparts (Fig. 2B).

Histopathological NASH assessment is typically based on scoring of steatosis, lobular inflammation and hepatocellular ballooning, included in the NAS [30]. Only statistically lower lobular inflammation ($p<0.05$) was found in Panx1$^{-/-}$ CHFD mice in comparison with the WT control (Fig. 3A). Serum ALT activity was elevated in WT CHFD mice (n=15) in comparison with WT ND mice ($p<0.001$) (n=10). This effect was diminished in Panx1$^{-/-}$ CHFD mice (n=12) compared to the WT counterparts ($p<0.001$). Serum AST activity was elevated in WT CHFD mice (n=15), but did not change in Panx1$^{-/-}$ CHFD animals (n=10) (Fig. 3B). All together, these data demonstrate that genetic ablation of Panx1 alleviates clinical hallmarks of liver injury both in acute liver failure and in NASH.

3.3 Effects of Panx1 deficiency on liver protein adduct formation

Under therapeutic doses, the formation of NAPQI, as a result of APAP bio-activation, can be rapidly detoxified by binding to GSH. However, in case of APAP overdosing, NAPQI reacts with protein sulfhydryl groups, which leads to the formation of liver protein adducts [14]. Accordingly, 1 hour after overdosing, APAP protein adducts were already detectable in WT and Panx1$^{-/-}$ mice. Interestingly, lower amounts of hepatic protein adducts were found after 1 ($p<0.01$) and 6 hours ($p<0.05$) of APAP administration in Panx1$^{-/-}$ mice (n=7) in comparison with WT animals (n=7) (Fig. 4A). These results indicate a lower metabolic

activity upon genetic ablation of Panx1 in the APAP mouse model. This was confirmed by the observation of lower ($p<0.01$) Cyp2e1 protein steady-state levels in Panx1$^{-/-}$ mice (n=5) (Fig. 4B).

3.4 Effects of Panx1 deficiency on liver oxidative stress

In this study, a gradual recovery of the total GSH pool became evident 6 and 24 hours after APAP administration in both experimental groups. The Panx1$^{-/-}$ mice (n=10) showed decreased amounts of the oxidized GSSG ($p<0.01$), resulting in lowered oxidative stress after 24 hours ($p<0.05$) (Fig. 4C). GR ($p<0.01$), GPx ($p<0.05$) and catalase ($p<0.01$) levels were elevated in Panx1$^{-/-}$ CHFD mice (n=11) in comparison with WT counterparts (n=15) (Fig. 5A). In order to complement the anti-oxidative enzyme activity data, protein expression of SOD, GR, GPx and catalase was studied. GR protein levels showed a significant increase in WT CHFD mice ($p<0.01$) and in Panx1$^{-/-}$ ND mice ($p<0.01$) in comparison with WT ND animals, while GPx protein quantities were upregulated in Panx1$^{-/-}$ CHFD mice ($p<0.01$) compared to WT CHFD animal and in Panx1$^{-/-}$ ND mice ($p<0.001$) compared to WT ND animals (Fig. 5B). This indicates that Panx1 affects oxidative stress in NASH and APAP-induced acute liver failure.

3.5 Effects of Panx1 deficiency on serum and liver lipids

Higher amounts of liver triglycerides ($p<0.001$) and cholesterol ($p<0.001$) were observed in WT CHFD mice (n=16) in comparison with WT ND animals (n=10). Panx1 deficiency (n=12) reduced liver cholesterol almost to baseline levels ($p<0.001$) in comparison with WT CHFD mice, while liver triglycerides were unaffected. Serum triglycerides were decreased in WT CHFD mice ($p<0.001$) (n=15), whereas an increase was found in Panx1$^{-/-}$ mice fed a ND ($p<0.01$) (n=12) in comparison with ND-fed WT animals (n=10) (Fig. 6). Overall, this suggests that genetic ablation of Panx1 alleviates liver cholesterol levels in NASH.

3.6 Effects of Panx1 deficiency on liver inflammatory markers

Of the 40 tested inflammatory markers, only 4 proteins were upregulated in WT APAP mice (n=3) (Table 2 and Fig. 7) compared to untreated WT animals. No changes were detected in Panx1$^{-/-}$ APAP mice (n=3) in comparison with the WT APAP group (n=3). In WT CHFD mice (n=3), levels of a number of tested inflammatory markers were increased in comparison with WT ND mice (n=3). These changes were reversed to baseline levels in Panx1$^{-/-}$ CHFD mice (n=3) (Table 2 and Fig. 8), showing that Panx1 deficiency resolves inflammation in NASH.

3.7 Effects of Panx1 deficiency on the liver transcriptome in APAP mice

In order to identify genes and pathways affected by genetic Panx1 deletion, whole transcriptome analysis was performed on liver tissue in the APAP mouse model. As such, 680 genes were significantly differentially expressed in WT APAP mice (n=5) in comparison with WT untreated animals (n=5). The most important modified pathways include genes involved in Cyp oxidation, mitogen-activated protein kinase signaling, protein-protein interactions, chemokine signaling and oxidative stress. In Panx1$^{-/-}$ mice (n=5), the expression of 1204 genes was statistically altered upon treatment with APAP,

among which 307 genes were also differently expressed in the WT APAP group (n=5) in comparison with the WT untreated group (n=5) (Fig. 9A). Of these, *Lect2, Alcam, Pvr, S100a9, S100a8, Ifrd1, Cxcl9* and *Cxcl1* are associated with neutrophil recruitment or activation, and were mostly upregulated in Panx1$^{-/-}$ APAP mice. Oxidative stress-related genes, such as *Ppm1k, Cisd1, Gpx1, Cyp4a12b, Cyp4a12a* and *Cyp3a25,* were mainly upregulated in Panx1$^{-/-}$ APAP mice, which is in contrast to the lower oxidized GSSG levels found in Panx1$^{-/-}$ APAP mice. However, *Gpx1*, coding for the anti-oxidative enzyme GPx, is involved in the reduction of hydrogen peroxide through the dismutation of superoxide anions or organic hydroperoxides. In this way, GPx is an important enzyme in the scavenging of ROS and the regulation of GSH and GSSG [39]. The upregulated RNA levels of *Gpx1* are therefore in line with the decreased GSSG levels seen in Panx1$^{-/-}$ APAP mice. Moreover, several genes playing a role in the biotransformation of xenobiotics, including *Ugt2a3, Ugt2b34, Ugt3a2, Ugt2b1, Ugt3a1, Ces3a, Ces1g, Ces3b* and *Ces1e,* showed higher expression levels in Panx1$^{-/-}$ APAP mice (Supplementary Table 1). For validation purposes, RNA expression levels of 3 differentially affected genes were tested with RT-qPCR analysis. As such, *Cd68* expression was increased ($p<0.001$) in WT APAP mice, while *Cxcl9* expression was decreased ($p<0.01$) in comparison with WT untreated mice. In Panx1$^{-/-}$ APAP mice, *Cd36* ($p<0.05$) and *Cd68* ($p<0.001$) RNA levels were downregulated and *Cxcl9* ($p<0.001$) RNA levels were upregulated ($p<0.05$) (Fig. 9B).

3.8 Effects of Panx1 deficiency on the liver transcriptome in NASH mice

In order to identify genes and pathways affected by genetic Panx1 deletion, whole transcriptome analysis was performed on liver tissue in the NASH mouse model. A total of 338 genes were differentially expressed in WT CHFD mice (n=5) in comparison with WT ND littermates (n=5). The most prominent pathway affected related to the biosynthesis of cholesterol, which shows strongly downregulated genes. This is in line with the elevated cholesterol levels in WT mice fed a CHFD. Other relevant pathways involved include peroxisome proliferator-activated receptor signaling, which exhibits mainly upregulated genes, insulin signaling, Cyp oxidation, mitogen-activated protein kinase signaling and adipocyte differentiation. In the liver of Panx1$^{-/-}$ CHFD mice (n=5), a total of 172 genes were differentially expressed in comparison with WT CHFD animals, of which 75 genes were also affected in the WT CHFD group in comparison with the WT ND group (Fig. 10A). Of these, *Cidec, Fasn, Cd36, Apoa4, Lpl, Lipg, Elovl3, Elovl6, Fabp7* and *Hmgcs1* are associated with lipid metabolism and were all downregulated in Panx1$^{-/-}$ CHFD mice. Genes involved in the inflammatory response, such as *Clec7a, Lcn2, Mt2, Cxcl9, Cd68, C1qb, Lilrb4a, Ly6a, Fcer1g, Vim, C3ar1, Tlr13* and *Ifi30,* were downregulated in Panx1$^{-/-}$ CHFD mice (Supplementary Table 2). Among those, Cxcl9 was also decreased at the protein level. For validation purposes, the RNA expression levels of 3 differentially affected genes were tested with RT-qPCR analysis. *Cd36* ($p<0.001$), *Cd68* ($p<0.001$) and *Cxcl9* ($p<0.05$) RNA quantities were increased in WT CHFD mice in comparison with WT ND mice. In Panx1$^{-/-}$ CHFD mice, *Cd36* ($p<0.01$), *Cd68* ($p<0.05$) and *Cxcl9* ($p<0.05$) RNA levels were downregulated in comparison with WT CHFD animals (Fig. 10B).

4. Discussion

In 1974, Goodenough isolated 2 gap junction proteins from mouse liver, which were designated connexins [40], of which 20 members in rodents and 21 in human are known today. Panx proteins were discovered in 2000 as connexin-like proteins, but gained a rapid increasing interest because of their role in cell death and inflammation [41–44]. It is now becoming clear that Panx channels can have physiological as well as pathological functions [41, 43]. In liver, Panx1 channels were found to play a role in experimentally induced lipo-apoptosis in hepatocytes [45] and APAP-induced acute liver failure in mice [11]. In this study, it was found that Panx1 RNA is detectable in healthy mouse HSCs, hepatocytes and Kupffer cells, but not in LSECs. Panx1 RNA levels were elevated both in experimental NASH as well as in acute liver failure in mice, which is in line with previous studies [11, 45]. Panx1$^{-/-}$ mice either fed a CHFD or overdosed with APAP were partially protected against experimentally induced NASH or acute liver failure, respectively, compared to WT cohorts, as evidenced by lower serum ALT and AST activities. Moreover, decreased levels of cholesterol, GR, GPx and catalase were observed in the liver of Panx1$^{-/-}$ CHFD mice, while lower levels of GSSG and GSSG/GSH were found in the liver of Panx1$^{-/-}$ APAP mice. However, it can not be fully excluded that part of the reduction in APAP-mediated injury in Panx1$^{-/-}$ mice is due to decreased bio-activation of APAP through lower levels of Cyp2e1. Indeed, lower levels of APAP-protein adducts were found 1 and 6 hours after APAP-administration in Panx1$^{-/-}$ mice compared to WT animals, which might question the suitability of these knock-out animals as a model to explore the effect of Panx1 in APAP-induced acute liver failure. However, the results of this study are similar to a previous study from our group in which pharmacological inhibition of Panx1 channels 1.5 hours after APAP-administration showed protective effects against acute liver failure [11]. Using this approach, a possible effect of Panx1 channel inhibition on APAP-protein adduct formation, and the model as such, could be ruled out. Therefore, one could assume that the protective effect of Panx1 deletion is not only due to the reduced amount of APAP-protein adducts, but also involves participation of Panx1 in the propagation of liver injury after APAP overdosing. Yet, protein expression of a number of inflammatory markers, such as IL-1α IL-1β, IL-2, IL-4, IL-7, IL-9, IL-17, leptin and IFN-γ, was decreased upon Panx1 deficiency in NASH, but not in acute liver failure.

In order to study the molecular mechanisms underlying these protective effects, whole transcriptome analysis was performed on liver tissue of CHFD and APAP WT and Panx1$^{-/-}$ mice. In Panx1$^{-/-}$ APAP mice, a number of genes linked to xenobiotic biotransformation, oxidative stress and inflammation were differentially expressed, of which *Lect2* [46] *Cxcl9* [47] *Cxcl1* [48] and *C1ra, Css2, C1rb, C1s1 C2, C6, C9* [49] are involved in acute liver failure. Indeed, complement activation has been shown to drive hepatic inflammation and progression of injury during the pathogenesis of APAP-induced acute liver failure [49]. *Lcn2* codes for the lipocalin 2 protein, a neutrophil pro-inflammatory factor causally involved in obesity-related metabolic and cardiovascular complications [50]. Lcn2 is usually expressed by leukocytes, but can be present in hepatic parenchymal cells upon inflammatory stress [51]. Cxcl9 is a chemotactic agent for T-cells and natural killer cells, yet can also be elevated after stimulation of neutrophils and hepatocytes by IL-γ [52]. Several genes associated with

lipid metabolism, inflammation and oxidative stress were found to be differentially changed in Panx1$^{-/-}$ CHFD mice. This is in line with the tested clinically relevant read-outs, since less cholesterol, inflammation and oxidative stress were found in Panx1$^{-/-}$ mice. Of those genes, *Cd36*, coding for an important protein in the transportation of fatty acids into cells, such as monocytes/macrophages, smooth muscle cells, Kupffer cells and stellate cells, was upregulated in WT CHFD mice, but downregulated in Panx1$^{-/-}$ CHFD mice. CD36 plays a central role in NASH [53], as its expression is elevated in *ob/ob* mice, *db/db* mice and mice fed a high-fat diet [54]. Other lipid-related genes include *Apoa4* [55] *Lpl* [56] *Elovl3* [57] *Elovl6* [58], *Cidec* [59] and *Hmgsc1* [60], which have all been shown to be involved in the pathogenesis of NASH. In fact, downregulated *Hmgsc1* expression correlates with the lower liver cholesterol levels found in Panx1$^{-/-}$ mice, since hydroxymethylglutaryl-coenzyme A synthase is an important enzyme in the synthesis of cholesterol. Genes both affected in CHFD and APAP Panx1$^{-/-}$ mice included *Cd68, Cxcl9, Elovl3, Hmgcs1, Lcn2, Vim, Cyp3a25* and *Cyp3a57*. It is therefore plausible that these genes and/or their corresponding proteins are important mediators in Panx1-associated liver disease. However, it still needs to be determined if these gene changes result from direct or indirect effects of genetic deletion of Panx1 [61]. Since whole-body Panx1 knock-out mice have been used in this study, it can as such not be excluded that Panx1 in other tissues, such as adipose tissue, pancreas or gut, affect liver disease pathogenesis. Analysis of The Human Metabolome Database reveals that there are over 35000 biological molecules that could theoretically pass through Panx1 channels [62]. Out of these signals, ATP is by far the most studied molecule, as it has been linked to the inflammatory response with T-cell activation and neutrophil recruitment through purinergic signaling [12, 63, 64]. In conclusion, Panx1 seems to play an important role in experimental acute and chronic liver disease, which is worth investigating in other liver diseases and in human patients.

Conclusion

These results suggest that Panx1 may play an important role in the pathogenesis of acute and chronic liver diseases.

Supplementary Material

Refer to Web version on PubMed Central for supplementary material.

Acknowledgments

This work was financially supported by the grants of the Agency for Innovation by Science and Technology in Flanders (IWT grant 131003), the University of São Paulo-Brazil, the Fundação de Amparo à Pesquisa do Estado de São Paulo (FAPESP SPEC grant 2013/50420-6, 2014/23890-4, 2014/23887-3 and 2016/03579-8), the European Research Council (ERC Starting Grant 335476), the Fund for Scientific Research-Flanders (FWO grants G009514N and G010214N), the National Institutes of Health (NIH grants DK102142, P20 GM103549 and R01 EY021517) and the University Hospital of the Vrije Universiteit Brussel-Belgium (“Willy Gepts Fonds” UZ-VUB).

Abbreviations

ALT	alanine aminotransferase
APAP	acetaminophen

AST	aspartate aminotransferase
ATP	adenosine triphosphate
BLC	B lymphocyte chemoattractant
CD30L	cluster of differentiation 30 ligand
CHFD	choline-deficient high-fat diet
Cyp2e1	cytochrome P450 2e1
GCSF	granulocyte colony-stimulating factor
(G)MCSF	(granulocyte)-macrophage colony-stimulating factor
GPx	glutathione peroxidase
GR	glutathione reductase
GSH	glutathione
GSSG	glutathione disulfide
HSCs	hepatic stellate cells
IFN	interferon
IL	interleukin
I-TAC	interferon-inducible T-cell α chemoattractant
LSECs	liver sinusoidal endothelial cells
MCP	monocyte chemoattractant protein
MIG	monokine induced by interferon-γ
MIP	macrophage inflammatory protein
n	number of repeats
NALP3, NACHT	LRR and PYD domains-containing protein 3
NAFLD	non-alcoholic fatty liver disease
NAS	NAFLD activity score
NASH	non-alcoholic steatohepatitis
ND	normal diet
Panx	pannexin
p	probability
SDF	stromal cell-derived factor

SEM	standard error of mean
SOD	superoxide dismutase
sTNFR	soluble tumor necrosis factor receptor
TCA	T-cell activation protein
TECK	thymus-expressed chemokine
TIMP	metalloproteinase inhibitor
WT	wild-type.

References

1. Penuela S, Bhalla R, Gong XQ, Cowan KN, Celetti SJ, Cowan BJ, Bai D, Shao Q, Laird DW. Pannexin 1 and pannexin 3 are glycoproteins that exhibit many distinct characteristics from the connexin family of gap junction proteins. J Cell Sci. 2007; 120:3772–3783. [PubMed: 17925379]
2. Bruzzone R, Hormuzdi SG, Barbe MT, Herb A, Monyer H. Pannexins, a family of gap junction proteins expressed in brain. Proc Natl Acad Sci U S A. 2003; 100:13644–13649. [PubMed: 14597722]
3. Le Vasseur M, Lelowski J, Bechberger JF, Sin WC, Naus CC. Pannexin 2 protein expression is not restricted to the CNS. Front Cell Neurosci. 2014; 8:392. [PubMed: 25505382]
4. Wang N, De Bock M, Decrock E, Bol M, Gadicherla A, Vinken M, Rogiers V, Bukauskas FF, Bultynck G, Leybaert L. Paracrine signaling through plasma membrane hemichannels. Biochim Biophys Acta. 2013; 1828:35–50. [PubMed: 22796188]
5. Csak T, Ganz M, Pespisa J, Kodys K, Dolganiuc A, Szabo G. Fatty acid and endotoxin activate inflammasomes in mouse hepatocytes that release danger signals to stimulate immune cells. Hepatology. 2011; 54:133–144. [PubMed: 21488066]
6. Ganz M, Csak T, Nath B, Szabo G. Lipopolysaccharide induces and activates the Nalp3 inflammasome in the liver. World J Gastroenterol. 2011; 17:4772–4778. [PubMed: 22147977]
7. Pelegrin P, Surprenant A. Pannexin-1 mediates large pore formation and interleukin-1beta release by the ATP-gated P2X7 receptor. EMBO J. 2006; 25:5071–5082. [PubMed: 17036048]
8. Jian Z, Ding S, Deng H, Wang J, Yi W, Wang L, Zhu S, Gu L, Xiong X. Probenecid protects against oxygen-glucose deprivation injury in primary astrocytes by regulating inflammasome activity. Brain Res. 2016; 1643:123–129. [PubMed: 27154322]
9. Marina-García N, Franchi L, Kim YG, Miller D, McDonald C, Boons GJ, Núñez G. Pannexin-1-mediated intracellular delivery of muramyl dipeptide induces caspase-1 activation via cryopyrin/NLRP3 independently of Nod2. J Immunol. 2008; 180:4050–4057. [PubMed: 18322214]
10. Bao Y, Chen Y, Ledderose C, Li L, Junger WG. Pannexin 1 channels link chemoattractant receptor signaling to local excitation and global inhibition responses at the front and back of polarized neutrophils. J Biol Chem. 2013; 288:22650–22657. [PubMed: 23798685]
11. Maes M, McGill MR, da Silva TC, Abels C, Lebofsky M, Weemhoff JL, Tiburcio T, Veloso Alves Pereira I, Willebrords J, Crespo Yanguas S, Farhood A, Beschin A, Van Ginderachter JA, Penuela S, Jaeschke H, Cogliati B, Vinken M. Inhibition of pannexin1 channels alleviates acetaminophen-induced hepatotoxicity. Arch Toxicol. 2017; 91:2245–2261. [PubMed: 27826632]
12. Chekeni FB, Elliott MR, Sandilos JK, Walk SF, Kinchen JM, Lazarowski ER, Armstrong AJ, Penuela S, Laird DW, Salvesen GS, Isakson BE, Bayliss DA, Ravichandran KS. Pannexin 1 channels mediate 'find-me' signal release and membrane permeability during apoptosis. Nature. 2010; 467:863–867. [PubMed: 20944749]
13. Larson AM. Acetaminophen hepatotoxicity. Clin Liver Dis. 2007; 11:525–548. vi. [PubMed: 17723918]

14. McGill MR, Jaeschke H. Metabolism and disposition of acetaminophen: recent advances in relation to hepatotoxicity and diagnosis. Pharm Res. 2013; 30:2174–2187. [PubMed: 23462933]
15. Jaeschke H, McGill MR, Ramachandran A. Oxidant stress, mitochondria and cell death mechanisms in drug-induced liver injury: lessons learned from acetaminophen hepatotoxicity. Drug Metab Rev. 2012; 44:88–106. [PubMed: 22229890]
16. Xiao F, Waldrop SL, Bronk SF, Gores GJ, Davis LS, Kilic G. Lipoapoptosis induced by saturated free fatty acids stimulates monocyte migration: a novel role for Pannexin1 in liver cells. Purinergic Signal. 2015; 11:347–359. [PubMed: 26054298]
17. Bellentani S. The epidemiology of non-alcoholic fatty liver disease. Liver Int. 2017; 37(Suppl 1): 81–84. [PubMed: 28052624]
18. Schuppan D, Schattenberg JM. Non-alcoholic steatohepatitis: pathogenesis and novel therapeutic approaches. J Gastroenterol Hepatol. 2013; 28(Suppl 1):68–76.
19. Buzzetti E, Pinzani M, Tsochatzis EA. The multiple-hit pathogenesis of non-alcoholic fatty liver disease (NAFLD). Metabolism. 2016; 65:1038–1048. [PubMed: 26823198]
20. Bellanti F, Villani R, Facciorusso A, Vendemiale G, Serviddio G. Lipid oxidation products in the pathogenesis of non-alcoholic steatohepatitis. Free Radic Biol Med. 2017; 111:173–185. [PubMed: 28109892]
21. Liu W, Baker SS, Baker RD, Zhu L. Antioxidant mechanisms in nonalcoholic fatty liver disease. Curr Drug Targets. 2015; 16:1301–1314. [PubMed: 25915484]
22. Videla LA, Rodrigo R, Orellana M, Fernandez V, Tapia G, Quiñones L, Varela N, Contreras J, Lazarte R, Csendes A, Rojas J, Maluenda F, Burdiles P, Diaz JC, Smok G, Thielemann L, Poniachik J. Oxidative stress-related parameters in the liver of non-alcoholic fatty liver disease patients. Clin Sci (Lond). 2004; 106:261–268. [PubMed: 14556645]
23. Laurent A, Nicco C, Tran Van Nhieu J, Borderie D, Chéreau C, Conti F, Jaffray P, Soubrane O, Calmus Y, Weill B, Batteux F. Pivotal role of superoxide anion and beneficial effect of antioxidant molecules in murine steatohepatitis. Hepatology. 2004; 39:1277–1285. [PubMed: 15122756]
24. Ioannou GN. The role of cholesterol in the pathogenesis of NASH. Trends Endocrinol Metab. 2016; 27:84–95. [PubMed: 26703097]
25. Ioannou GN, Subramanian S, Chait A, Haigh WG, Yeh MM, Farrell GC, Lee SP, Savard C. Cholesterol crystallization within hepatocyte lipid droplets and its role in murine NASH. J Lipid Res. 2017; 58:1067–1079. [PubMed: 28404639]
26. Mridha AR, Wree A, Robertson AA, Yeh MM, Johnson CD, Van Rooyen DM, Haczeyni F, Teoh NC, Savard C, Ioannou GN, Masters SL, Schroder K, Cooper MA, Feldstein AE, Farrell GC. NLRP3 inflammasome blockade reduces liver inflammation and fibrosis in experimental NASH in mice. J Hepatol. 2017; 66:1037–1046. [PubMed: 28167322]
27. Mannaerts I, Schroyen B, Verhulst S, Van Lommel L, Schuit F, Nyssen M, van Grunsven LA. Gene expression profiling of early hepatic stellate cell activation reveals a role for Igfbp3 in cell migration. PLoS One. 2013; 8:e84071. [PubMed: 24358328]
28. Dvoriantchikova G, Ivanov D, Barakat D, Grinberg A, Wen R, Slepak VZ, Shestopalov VI. Genetic ablation of Pannexin1 protects retinal neurons from ischemic injury. PLoS One. 2012; 7:e31991. [PubMed: 22384122]
29. Gujral JS, Knight TR, Farhood A, Bajt ML, Jaeschke H. Mode of cell death after acetaminophen overdose in mice: apoptosis or oncotic necrosis? Toxicol Sci. 2002; 67:322–328. [PubMed: 12011492]
30. Kleiner DE, Brunt EM, Van Natta M, Behling C, Contos MJ, Cummings OW, Ferrell LD, Liu YC, Torbenson MS, Unalp-Arida A, Yeh M, McCullough AJ, Sanyal AJ, Network NSCR. Design and validation of a histological scoring system for nonalcoholic fatty liver disease. Hepatology. 2005; 41:1313–1321. [PubMed: 15915461]
31. Tiburcio TC, Willebrords J, da Silva TC, Pereira IV, Nogueira MS, Yanguas SC, Maes M, Silva ED, Dagli ML, de Castro IA, Oliveira CP, Vinken M, Cogliati B. Connexin32 deficiency is associated with liver injury, inflammation and oxidative stress in experimental non-alcoholic steatohepatitis. Clin Exp Pharmacol Physiol. 2016; 44:197–206.

32. McGill MR, Jaeschke H. A direct comparison of methods used to measure oxidized glutathione in biological samples: 2-vinylpyridine and N-ethylmaleimide. Toxicol Mech Methods. 2015; 25:589–595. [PubMed: 26461121]
33. Muldrew KL, James LP, Coop L, McCullough SS, Hendrickson HP, Hinson JA, Mayeux PR. Determination of acetaminophen-protein adducts in mouse liver and serum and human serum after hepatotoxic doses of acetaminophen using high-performance liquid chromatography with electrochemical detection. Drug Metab Dispos. 2002; 30:446–451. [PubMed: 11901099]
34. Goldberg GS, Moreno AP, Bechberger JF, Hearn SS, Shivers RR, MacPhee DJ, Zhang YC, Naus CC. Evidence that disruption of connexon particle arrangements in gap junction plaques is associated with inhibition of gap junctional communication by a glycyrrhetinic acid derivative. Exp Cell Res. 1996; 222:48–53. [PubMed: 8549672]
35. Willebrords J, Cogliati B, Pereira IVA, da Silva TC, Crespo Yanguas S, Maes M, Govoni VM, Lima A, Felisbino DA, Decrock E, Nogueira MS, de Castro IA, Leclercq I, Leybaert L, Rodrigues RM, Vinken M. Inhibition of connexin hemichannels alleviates non-alcoholic steatohepatitis in mice. Sci Rep. 2017; 7:8268. [PubMed: 28811572]
36. Livak KJ, Schmittgen TD. Analysis of relative gene expression data using real-time quantitative PCR and the 2(−Delta Delta C(T)) Method. Methods. 2001; 25:402–408. [PubMed: 11846609]
37. Sáez PJ, Shoji KF, Aguirre A, Sáez JC. Regulation of hemichannels and gap junction channels by cytokines in antigen-presenting cells. Mediators Inflamm. 2014; 2014:742734. [PubMed: 25301274]
38. Kim HY, Kim SJ, Lee SM. Activation of NLRP3 and AIM2 inflammasomes in Kupffer cells in hepatic ischemia/reperfusion. FEBS J. 2015; 282:259–270. [PubMed: 25327779]
39. Zitka O, Skalickova S, Gumulec J, Masarik M, Adam V, Hubalek J, Trnkova L, Kruseova J, Eckschlager T, Kizek R. Redox status expressed as GSH:GSSG ratio as a marker for oxidative stress in paediatric tumour patients. Oncol Lett. 2012; 4:1247–1253. [PubMed: 23205122]
40. Goodenough DA. Bulk isolation of mouse hepatocyte gap junctions. Characterization of the principal protein, connexin. J Cell Biol. 1974; 61:557–563. [PubMed: 4363961]
41. Crespo Yanguas S, Willebrords J, Johnstone SR, Maes M, Decrock E, De Bock M, Leybaert L, Cogliati B, Vinken M. Pannexin1 as mediator of inflammation and cell death. Biochim Biophys Acta. 2017; 1864:51–61. [PubMed: 27741412]
42. Maes M, Crespo Yanguas S, Willebrords J, Cogliati B, Vinken M. Connexin and pannexin signaling in gastrointestinal and liver disease. Transl Res. 2015; 166:332–343. [PubMed: 26051630]
43. Makarenkova HP, Shestopalov VI. The role of pannexin hemichannels in inflammation and regeneration. Front Physiol. 2014; 5:63. [PubMed: 24616702]
44. Mohammad M, Habib HS. Pannexin channels: the emerging therapeutic targets. Curr Drug Targets. 2014; 15:272–280. [PubMed: 24041333]
45. Xiao F, Waldrop SL, Khimji AK, Kilic G. Pannexin1 contributes to pathophysiological ATP release in lipoapoptosis induced by saturated free fatty acids in liver cells. Am J Physiol Cell Physiol. 2012; 303:C1034–1044. [PubMed: 22972801]
46. Sato Y, Watanabe H, Kameyama H, Kobayashi T, Yamamoto S, Takeishi T, Hirano K, Oya H, Nakatsuka H, Watanabe T, Kokai H, Yamagoe S, Suzuki K, Oya K, Kojima K, Hatakeyama K. Serum LECT2 level as a prognostic indicator in acute liver failure. Transplant Proc. 2004; 36:2359–2361. [PubMed: 15561249]
47. Wakabayashi H, Ito T, Fushimi S, Nakashima Y, Itakura J, Qiuying L, Win MM, Cuiming S, Chen C, Sato M, Mino M, Ogino T, Makino H, Yoshimura A, Matsukawa A. Spred-2 deficiency exacerbates acetaminophen-induced hepatotoxicity in mice. Clin Immunol. 2012; 144:272–282. [PubMed: 22868447]
48. Takada H, Mawet E, Shiratori Y, Hikiba Y, Nakata R, Yoshida H, Okano K, Kamii K, Omata M. Chemotactic factors released from hepatocytes exposed to acetaminophen. Dig Dis Sci. 1995; 40:1831–1836. [PubMed: 7648987]
49. Singhal R, Ganey PE, Roth RA. Complement activation in acetaminophen-induced liver injury in mice. J Pharmacol Exp Ther. 2012; 341:377–385. [PubMed: 22319198]

50. Wang Y. Small lipid-binding proteins in regulating endothelial and vascular functions: focusing on adipocyte fatty acid binding protein and lipocalin-2. Br J Pharmacol. 2012; 165:603–621. [PubMed: 21658023]
51. Ye D, Yang K, Zang S, Lin Z, Chau HT, Wang Y, Zhang J, Shi J, Xu A, Lin S. Lipocalin-2 mediates non-alcoholic steatohepatitis by promoting neutrophil-macrophage crosstalk via the induction of CXCR2. J Hepatol. 2016; 65:988–997. [PubMed: 27266617]
52. Semba T, Nishimura M, Nishimura S, Ohara O, Ishige T, Ohno S, Nonaka K, Sogawa K, Satoh M, Sawai S, Matsushita K, Imazeki F, Yokosuka O, Nomura F. The FLS (fatty liver Shionogi) mouse reveals local expressions of lipocalin-2, CXCL1 and CXCL9 in the liver with non-alcoholic steatohepatitis. BMC Gastroenterol. 2013; 13:120. [PubMed: 23875831]
53. Vinken M. The adverse outcome pathway concept: a pragmatic tool in toxicology. Toxicology. 2013; 312:158–165. [PubMed: 23978457]
54. Ge JF, Walewski JL, Anglade D, Berk PD. Regulation of hepatocellular fatty acid uptake in mouse models of fatty liver disease with and without functional leptin signaling: roles of NfKB and SREBP-1C and the effects of spexin. Semin Liver Dis. 2016; 36:360–372. [PubMed: 27997977]
55. Wu CL, Zhao SP, Yu BL. Intracellular role of exchangeable apolipoproteins in energy homeostasis, obesity and non-alcoholic fatty liver disease. Biol Rev Camb Philos Soc. 2015; 90:367–376. [PubMed: 24834836]
56. Chen Y, Huang H, Xu C, Yu C, Li Y. Long non-coding RNA profiling in a non-alcoholic fatty liver disease rodent model: new insight into pathogenesis. Int J Mol Sci. 2017; 18:pii E21.
57. Xu C, Wang G, Hao Y, Zhi J, Zhang L, Chang C. Correlation analysis between gene expression profile of rat liver tissues and high-fat emulsion-induced nonalcoholic fatty liver. Dig Dis Sci. 2011; 56:2299–2308. [PubMed: 21327921]
58. Matsuzaka T, Atsumi A, Matsumori R, Nie T, Shinozaki H, Suzuki-Kemuriyama N, Kuba M, Nakagawa Y, Ishii K, Shimada M, Kobayashi K, Yatoh S, Takahashi A, Takekoshi K, Sone H, Yahagi N, Suzuki H, Murata S, Nakamuta M, Yamada N, Shimano H. Elovl6 promotes nonalcoholic steatohepatitis. Hepatology. 2012; 56:2199–2208. [PubMed: 22753171]
59. Tanaka N, Takahashi S, Matsubara T, Jiang C, Sakamoto W, Chanturiya T, Teng R, Gavrilova O, Gonzalez FJ. Adipocyte-specific disruption of fat-specific protein 27 causes hepatosteatosis and insulin resistance in high-fat diet-fed mice. J Biol Chem. 2015; 290:3092–3105. [PubMed: 25477509]
60. Dai W, Wang K, Zheng X, Chen X, Zhang W, Zhang Y, Hou J, Liu L. High fat plus high cholesterol diet lead to hepatic steatosis in zebrafish larvae: a novel model for screening anti-hepatic steatosis drugs. Nutr Metab (Lond). 2015; 12:42. [PubMed: 26583037]
61. Kardami E, Dang X, Iacobas DA, Nickel BE, Jeyaraman M, Srisakuldee W, Makazan J, Tanguy S, Spray DC. The role of connexins in controlling cell growth and gene expression. Prog Biophys Mol Biol. 2007; 94:245–264. [PubMed: 17462721]
62. Esseltine JL, Laird DW. Next-generation connexin and pannexin cell biology. Trends Cell Biol. 2016; 26:944–955. [PubMed: 27339936]
63. Elliott MR, Chekeni FB, Trampont PC, Lazarowski ER, Kadl A, Walk SF, Park D, Woodson RI, Ostankovich M, Sharma P, Lysiak JJ, Harden TK, Leitinger N, Ravichandran KS. Nucleotides released by apoptotic cells act as a find-me signal to promote phagocytic clearance. Nature. 2009; 461:282–286. [PubMed: 19741708]
64. Dahl G, Qiu F, Wang J. The bizarre pharmacology of the ATP release channel pannexin1. Neuropharmacology. 2013; 75:583–593. [PubMed: 23499662]

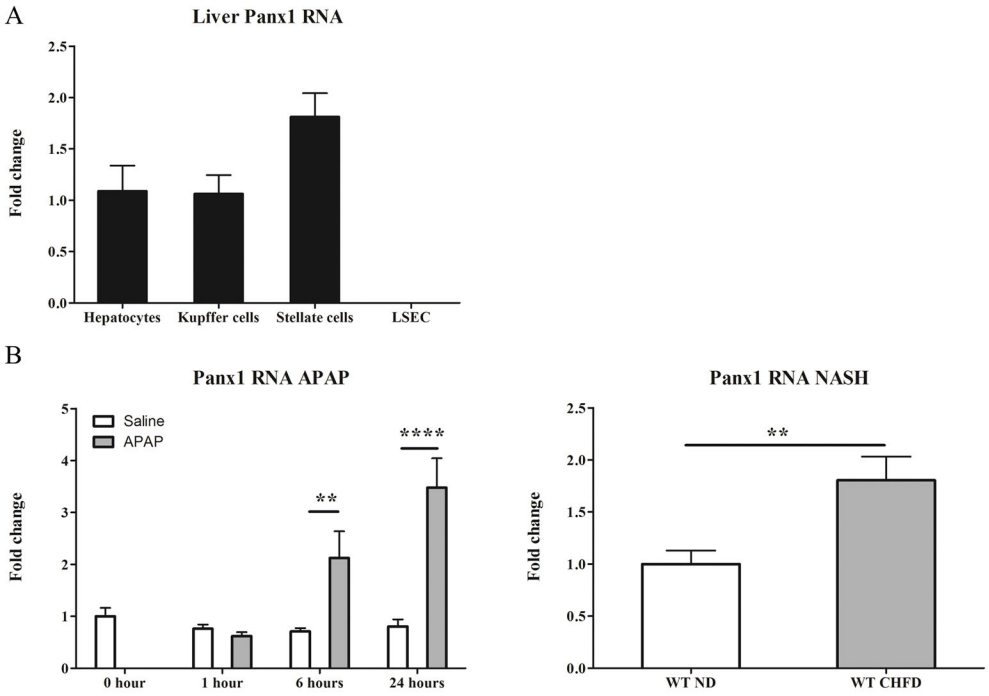

Figure 1. Panx1 expression in healthy and diseased liver

Stellate cells, LSECs, Kupffer cells and hepatocytes were isolated from the liver of untreated WT mice. WT mice were overdosed with APAP for 1, 6 or 24 hours or fed a CHFD (n=9) for 8 weeks. Panx1 RNA levels were measured in liver cells or tissue. **(A)** Panx1 RNA in stellate cells, LSECs, Kupffer cells and hepatocytes. **(B)** Panx1 RNA in liver tissue of WT CHFD and WT APAP mice. Data are expressed as means ± SEM with **p<0.01 and ****p<0.0001.

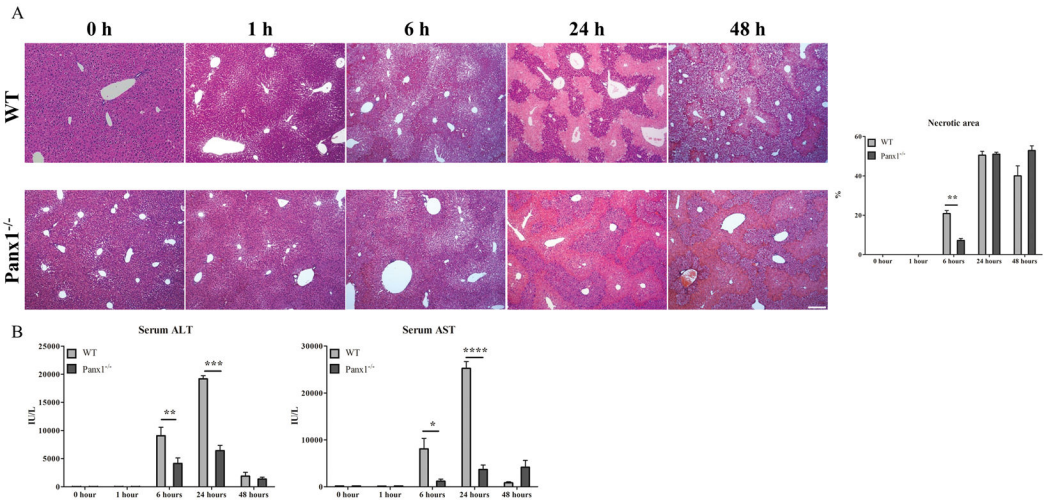

Figure 2. Effects of Panx1 deficiency on liver histology and injury in acute liver failure

WT and Panx1$^{-/-}$ mice were overdosed with APAP for 1, 6, 24 and 48 hours. **(A)** Necrotic areas were calculated for WT untreated, WT APAP, Panx1$^{-/-}$ untreated and Panx1$^{-/-}$ APAP mice. **(B)** Serum ALT and AST activity levels. Data are expressed as means ± SEM with *p<0.05, **p<0.01, ***p<0.001 and ****p<0.0001.

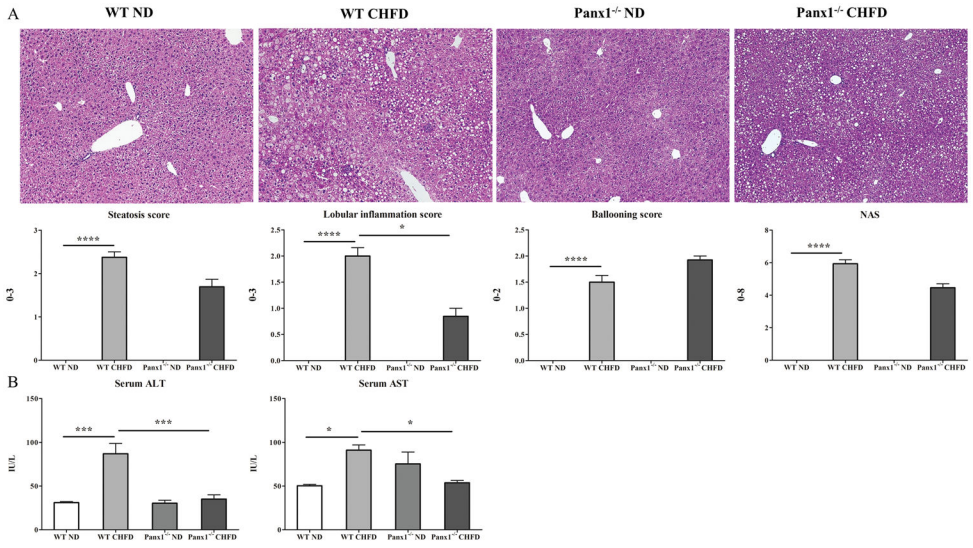

Figure 3. Effects of Panx1 deficiency on liver histology and injury in NASH

WT and Panx1$^{-/-}$ mice were fed a CHFD for 8 weeks. **(A)** Steatosis, lobular inflammation, ballooning score and NAS based on hematoxylin-eosin staining of liver tissue of WT ND, WT CHFD, Panx1$^{-/-}$ ND and Panx1$^{-/-}$ CHFD mice. **(B)** Serum ALT and AST activity levels. Data are expressed as means ± SEM with *p<0.05, ***p<0.001 and ****p<0.0001.

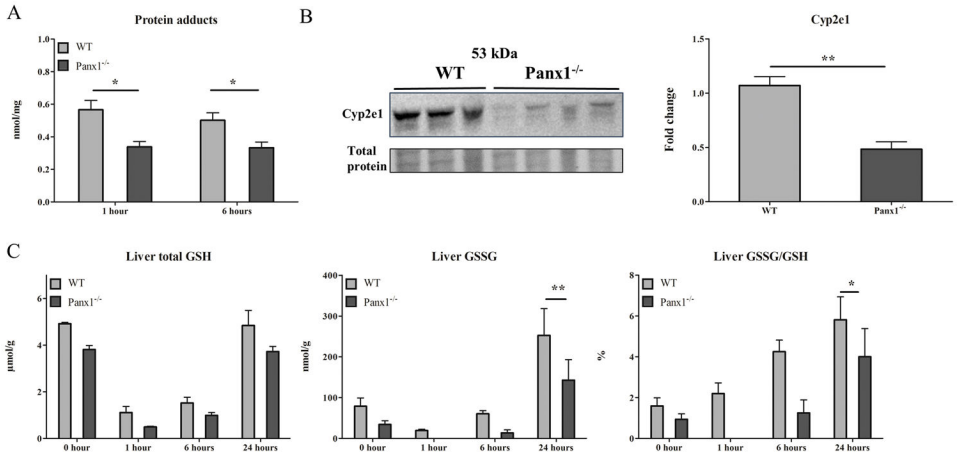

Figure 4. Effects of Panx1 deficiency on protein adducts and oxidative stress in acute liver failure

WT and Panx1$^{-/-}$ mice were overdosed with APAP for 1, 6 and 24 hours. **(A)** APAP-CYS protein adducts were quantified by high-pressure liquid chromatography with electrochemical detection using total liver homogenate. **(B)** Immunoblot analysis of Cyp2e1 (53 kDa) after separation and blotting, followed by normalization to total protein and expressed as fold change against normalized content of WT mice. (**C**) Liver GSH and GSSG levels. Data are expressed as means ± SEM with *p<0.05 and **p<0.01.

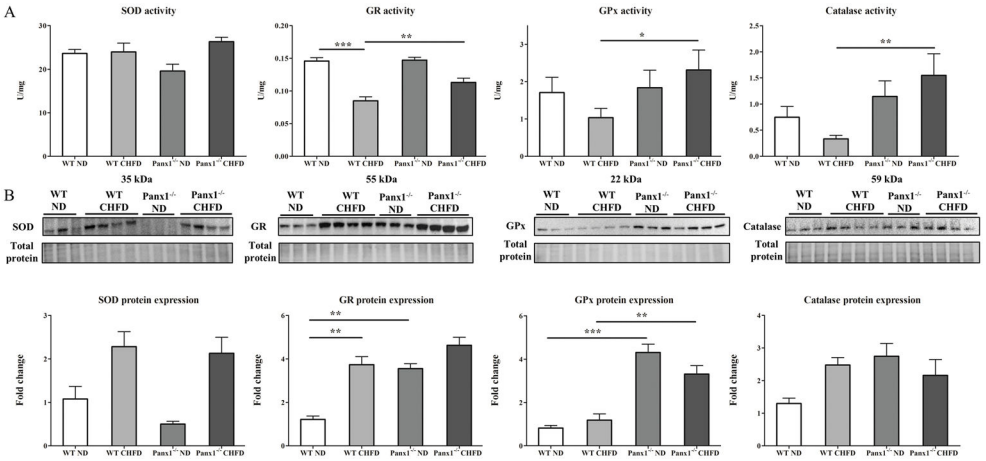

Figure 5. Effects of Panx1 deficiency on liver oxidative stress in NASH

WT and Panx1$^{-/-}$ mice were fed a CHFD for 8 weeks. **(A)** GR, GPx, catalase and SOD activity levels were measured. (**B**) Immunoblot analysis of SOD (35 kDa), GR (55 kDa), GPx (22 kDa) and catalase (59 kDa) after separation and blotting, followed by normalization to total protein and expressed as fold change against normalized content of WT ND mice. Data are expressed as means ± SEM with *p<0.05, **p<0.01 and ***p<0.001.

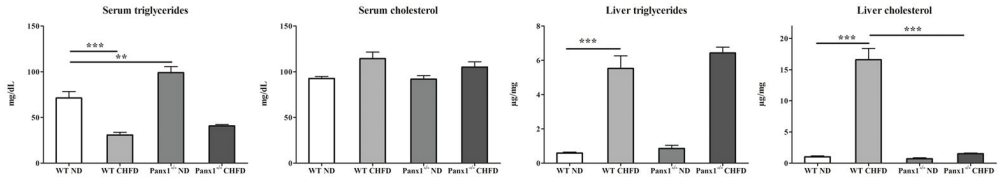

Figure 6. Effects of Panx1 deficiency on liver lipids in NASH

WT and Panx1$^{-/-}$ mice were fed a CHFD for 8 weeks. Serum and liver triglycerides and cholesterol levels were measured. Data are expressed as means ± SEM with **p<0.01 and ***p<0.001.

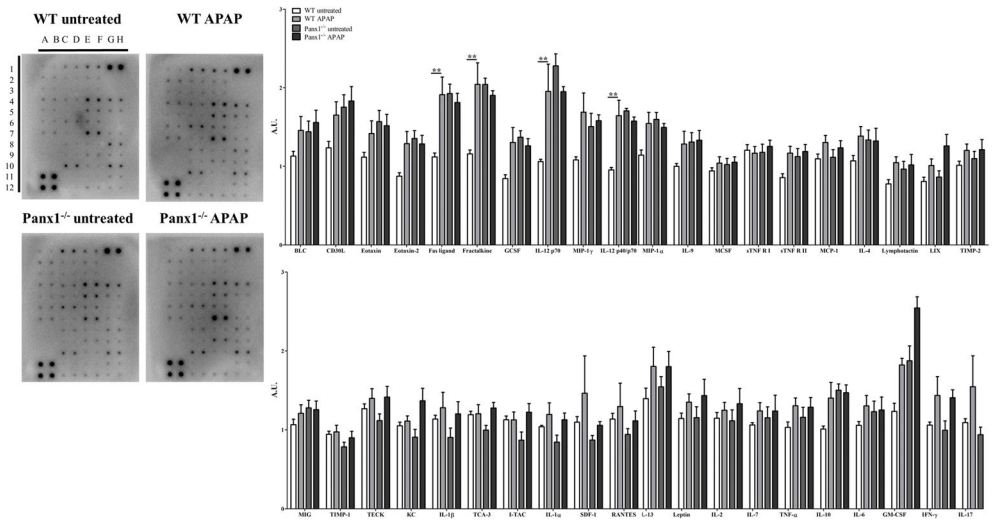

Figure 7. Effects of Panx1 deficiency on liver inflammatory markers in acute liver failure

WT and Panx1$^{-/-}$ mice were overdosed with APAP for 24 hours. Antibody array blots of protein extracts from liver tissue of WT untreated, WT APAP, Panx1$^{-/-}$ untreated and Panx1$^{-/-}$ APAP mice. Data were analyzed by densitometric analysis and were normalized to the average of the positive controls. Data are expressed as means ± SEM with **p<0.01. (BLC, B lymphocyte chemoattractant; CD30L, cluster of differentiation 30 ligand; GCSF, granulocyte colony-stimulating factor; (G)MCSF, (granulocyte)-macrophage colony-stimulating factor; IFN, interferon; IL, interleukin, I-TAC, interferon-inducible T-cell α chemoattractant; MCP, monocyte chemoattractant protein; MIG, monokine induced by interferon-γ; MIP, macrophage inflammatory protein; SDF, stromal cell-derived factor; sTNFR, soluble tumor necrosis factor receptor; TCA, T-cell activation protein; TECK, thymus-expressed chemokine; TIMP, metalloproteinase inhibitor).

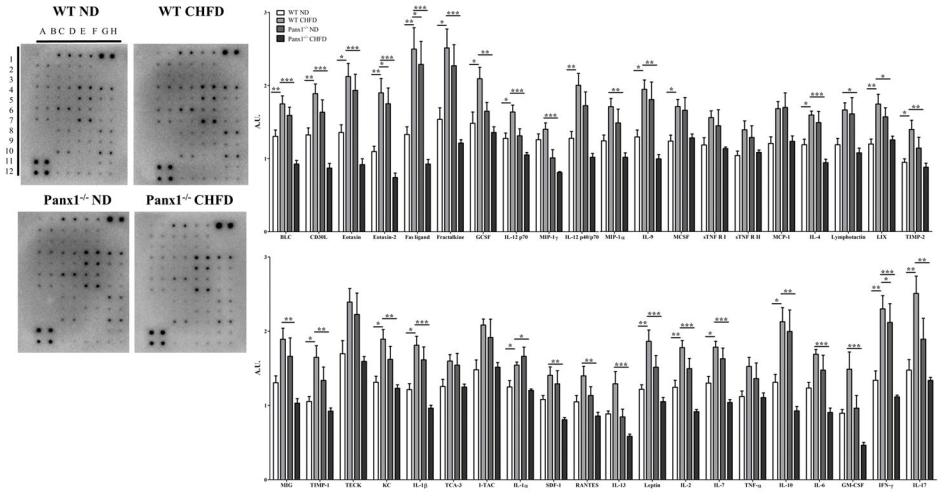

Figure 8. Effects of Panx1 deficiency on liver inflammatory markers in NASH

WT and Panx1$^{-/-}$ mice were fed a CHFD for 8 weeks. Antibody array blots of protein extracts from liver tissue of WT ND, WT CHFD, Panx1$^{-/-}$ ND and Panx1$^{-/-}$ CHFD mice. Data were analyzed by densitometric analysis and were normalized to the average of the positive controls. Data are expressed as means ± SEM with *p<0.05, **p<0.01 and ***p<0.001. (BLC, B lymphocyte chemoattractant; CD30L, cluster of differentiation 30 ligand; GCSF, granulocyte colony-stimulating factor; (G)MCSF, (granulocyte)-macrophage colony-stimulating factor; IFN, interferon; IL, interleukin, I-TAC, interferon-inducible T-cell α chemoattractant; MCP, monocyte chemoattractant protein; MIG, monokine induced by interferon-γ; MIP, macrophage inflammatory protein; SDF, stromal cell-derived factor; sTNFR, soluble tumor necrosis factor receptor; TCA, T-cell activation protein; TECK, thymus-expressed chemokine; TIMP, metalloproteinase inhibitor).

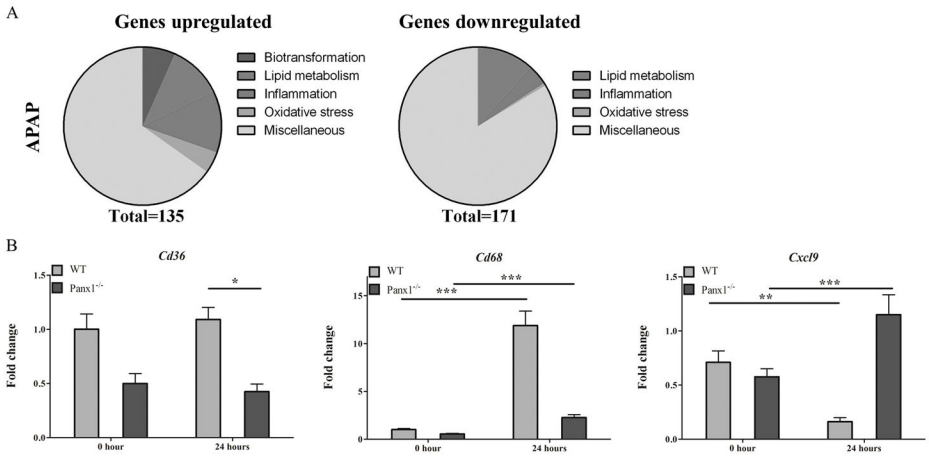

Figure 9. Effects of Panx1 deficiency on the liver transcriptome in acute liver failure

WT and Panx1$^{-/-}$ mice were overdosed with APAP for 24 hours. (**A**) The number of upregulated and downregulated genes represent affected genes in Panx1$^{-/-}$ mice in comparison with WT counterparts. (**B**) Gene expression levels of *Cd36*, *Cd68* and *Cxcl9.* Data are expressed as means ± SEM with *p<0.05, **p<0.01 and ***p<0.001.

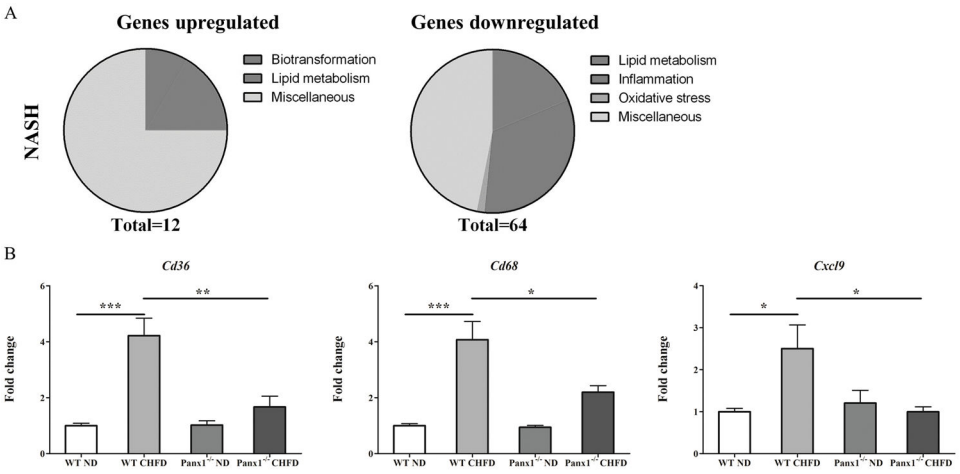

Figure 10. Effects of Panx1 deficiency on the liver transcriptome in NASH

WT and Panx1$^{-/-}$ mice were fed a CHFD for 8 weeks. (**A**) The number of upregulated and downregulated genes represent affected genes in Panx1$^{-/-}$ mice in comparison with WT counterparts. (**B**) Gene expression levels of *Cd36*, *Cd68* and *Cxcl9.* Data are expressed as means ± SEM with *p<0.05, **p<0.01 and ***p<0.001.

Table 1

Primers used for gene expression analysis

(*Actb*, actin β; *B2m*, β-2-microglobulin; *Gapdh*, glyceraldehyde 3-phosphate dehydrogenase; *Hmbs*, hydroxymethylbilane synthase; *Panx1*, pannexin1; *Ubc*, ubiquitin C).

Gene	Assay ID	Accession number	Assay location	Amplicon size (base pairs)	Exon boundary
Panx1	Mm00450900_m1	NM_019482.2	986	70	3–4
Cd36	Mm00432403_m1	NM_001159555.1	1214	104	8–9
Cd68	Mm03047343_m1	NM_001291058.1	956	109	5–6
Cxcl9	Mm00434946_m1	NM_008599.4	243	64	2–6
Actb	Mm00607939_s1	NM_007393.3	1233	115	6–6
B2m	Mm00437762_m1	NM_009735.3	111	77	1–2
Gapdh	Mm99999915_g1	NM_008084.2	265	107	2–3
Hmbs	Mm01143545_m1	NM_013551.2	473	81	6–7
Ubc	Mm02525934_g1	NM_019639.4	370	176	2–2

Table 2

Protein positions on blot

(BLC, B lymphocyte chemoattractant; CD30L, cluster of differentiation 30 ligand; GCSF, granulocyte colony-stimulating factor; (G)MCSF, (granulocyte)-macrophage colony-stimulating factor; IFN, interferon; IL, interleukin, I-TAC, interferon-inducible T-cell α chemoattractant; MCP, monocyte chemoattractant protein; MIG, monokine induced by interferon-γ; MIP, macrophage inflammatory protein; SDF, stromal cell-derived factor; sTNFR, soluble tumor necrosis factor receptor; TCA, T-cell activation protein; TECK, thymus-expressed chemokine; TIMP, metalloproteinase inhibitor).

Position on blot	Protein name	Position on blot	Protein name
A1/B1	**GCSF**	A7/B7	**BLC**
C1/D1	**IL-12 p70**	C7/D7	**IL-7**
E1/F1	**MIP-1γ**	E7/F7	**LIX**
G1/H1	**Positive control**	G7/H7	**TIMP-2**
A2/B2	**Fractalkine**	A8/B8	**Blank**
C2/D2	**IL-12 p40/p70**	C8/D8	**IL-2**
E2/F2	**MIP-1α**	E8/F8	**Leptin**
G2/H2	**Blank**	G8/H8	**TIMP-1**
A3/B3	**Fas ligand**	A9/B9	**Negative control**
C3/D3	**IL-10**	C9/D9	**IL-1β**
E3/F3	**MIG**	E9/F9	**KC**
G3/H3	**Blank**	G9/H9	**TECK**
A4/B4	**Eotaxin-2**	A10/B10	**Negative control**
C4/D4	**IL-9**	C10/D10	**IL-1α**
E4/F4	**MCSF**	E10/F10	**I-TAC**
G4/H4	**sTNF R II**	G10/H10	**TCA-3**
A5/B5	**Eotaxin**	A11/B11	**Positive control**
C5/D5	**IL-6**	C11/D11	**IFN-γ**
E5/F5	**MCP-1**	E11/F11	**IL-17**
G5/H5	**sTNFRI**	G11/H11	**SDF-1**
A6/B6	**CD30L**	A12/B12	**Positive control**
C6/D6	**IL-4**	C12/D12	**GM-CSF**
E6/F6	**Lymphotactin**	E12/F12	**IL-13**
G6/H6	**TNF-α**	G12/H12	**RANTES**